A Source or a Sink? How the Altitude of Particle Precipitation Influence High-Latitude Electrodynamics

Magnus F Ivarsen[1,2]

[1]Department of Physics and Engineering Physics, University of Saskatchewan, Saskatoon, Canada
[2]The European Space Agency Centre for Earth Observation, Frascati, Italy

Correspondence: magnus.fagernes@gmail.com

Abstract. From the sum total dissipation of unstable wave energy in geospace, a frequent and efficient channel of dissipation is opened up by particle precipitation. The phenomenon, which is part of a complicated cascade of unstable magnetohydrodynamic wave modes, consist of charged particles that intermittently rain down into Earth's dense atmosphere. The atmospheric penetration depth of the precipitating particles in aurorae dictates the altitude profile of plasma ionization. Absent of sunlight, this profile governs the crucial ratio of bottomside- to topside (E- to F-region) electrical conductance, which can act as a primary regulator of plasma turbulence growth rates by modulating the efficiency of electric field short-circuiting as well as ambipolar diffusion. Analyzing a large database of DMSP particle spectra from the dark, high-latitude ionosphere, we systematically map the response of this conductance ratio to varying geomagnetic activity. We reveal a characteristic spatial organization: during active conditions, the dayside cusp region is systematically drained of high-energy particles, creating a low-conductivity environment that favors the persistence of F-region turbulence, which starkly contrasts with the nightside auroral oval where elevated Pedersen conductivity in the E-region may actively dampen the growth of turbulence in the F-region. These findings indicate that the specific character of the magnetospheric energy input shapes the electrodynamics of specific regions, with implications for whether the ionosphere acts as a source or a sink for small-scale structuring.

1 Introduction

The most prominent feature of geospace, Earth's space environment, is the constant pushing of the solar wind against Earth's extended magnetic presence, the magnetosphere (Cowley, 2000). A basic two-cell convection pattern forms in the ionosphere at high latitudes, inside which plasma drifts, or convects, from the dayside to the nightside (Thomas and Shepherd, 2018). This large-scale drift of plasma essentially envelops geospace.

Inherent to this large-scale pattern is a complex energy cascade that originates in magnetospheric wave energy, starting with solar-wind-driven waves at the bow shock or magnetopause generating the ubiquitous ultra-low frequency (ULF) waves that traverse the magnetosphere (Krämer et al., 2024; Ivarsen et al., 2025d). The unstable wave energy fulfills many roles in the system. Central to the present paper, they ultimately power the regions of structured, periodic high-energy charged particle precipitation in the ionosphere's auroral regions (Newell et al., 2009, 2010; Thorne et al., 2010; Kasahara et al., 2018); this flux of charged particles carries (on account of being electrons) electrical currents as well as a Poynting flux, the transfer of

electromagnetic energy. At the same time, ULF waves produce a considerable Alfvénic Poynting flux directly, wherein the interchange instability (Huba et al., 1985; Keskinen and Huba, 1990; Greene et al., 2025) and the Alfvén wave resonator cavity (Lysak, 1991; Knudsen et al., 1990) transports electromagnetic energy downwards into Earth's atmosphere, where it eventually dissipates by heating up the gas. Alfvén waves experience anomalous resistivity and accelerate electrons, producing aurorae (Borovsky et al., 2019; Lysak et al., 2020). The total energy expenditure of the above constitute an important driver of electrodynamics in the ionosphere (Keiling et al., 2003; Sibeck and Murphy, 2025; Watanabe et al., 2025).

Common for the ways in which unstable wave energy is spent in the ionosphere-thermosphere system, all work crucial modulations into ionospheric conductivity and the electric fields that penetrate geospace, which in turn drives plasma dynamics directly and through particle precipitation, and this includes the essentially regulating role of the system on occurrences of small-scale structuring of the auroral ionosphere. As mentioned, this regulation occurs through modulations to electric fields (Hosokawa et al., 2008; Ivarsen et al., 2024b) and conductivities (Robinson et al., 2021; Hosokawa et al., 2010a), providing driving and damping effects for the triggering of plasma instabilities and subsequent growth of small-scale turbulent structuring within the plasma (Tsunoda, 1988; Vickrey and Kelley, 1982; Ivarsen et al., 2019), instabilities that are otherwise contributing to Landau damping at higher altitudes.

In addition, the *embedding* of a wave-cascade, or 'structural imprint' into the ionospheric plasma (Rinnert, 1992; Ivarsen et al., 2024a, 2025b), has been evoked to explain observations of density irregularities that appear directly driven by magnetospheric processes (Shen et al., 2024; Ivarsen et al., 2024a, 2025a), representing kinetic-scale Alfvénic turbulence (Greene et al., 2025) that is imprinted into the fields (see also David and Galtier, 2019; Borovsky, 2012).

1.1 Motivation

Our motivation stems from the important damping effects of elevated ionospheric conductance (Dimant et al., 2021), includes the boundary effects imposed by current continuity and the canceling of fields by currents that strive to achieve neutralization, but also through the accelerated diffusion facilitated by increased charge carrier mobility. An example of the effect can be readily demonstrated in the data: the main ionization source for the ionosphere is the Sun, whose extreme ultraviolet (EUV) radiation maintains a strong, steady-state, partial (< 1 %) ionization of the entire dayside atmosphere. The factor of importance in the case of solar EUV radiation is the solar zenith angle, the angle between Earth's surface and a vector connecting the observer to the centre of our Sun, Z, as well as the $F_{10.7}$-index, the quantified 10.7 cm solar radio flux (Moen and Brekke, 1993). Figure 1d–f) show the estimated conductance of the ionosphere in three seasonal bins, highlighting how the turning of the seasons lead to drastic changes to the ionosphere's ability to support currents, and Figure 1a–c) demonstrate the effects of conductance in smoothing out plasma density gradients (Ivarsen et al., 2023).

That is, Figure 1a–c) show the occurrence rate of radio phase fluctuations above Svalbard, Norway, for the same three seasonal bins. Such disturbances, called GNSS (Global Navigational Satellite System) phase fluctuations, are refraction of the radio signal (Wang et al., 2018; McCaffrey and Jayachandran, 2019; Spogli et al., 2021; Ghobadi et al., 2020; Conroy et al., 2022; Wang et al., 2022) as the signal passes through kilometer-scale gradients in plasma density (Song et al., 2023; Meziane et al., 2023), or, more generally, plasma density irregularities (Yeh and Liu, 1982; Kintner P. M. et al., 2007; Jin et al., 2017). In
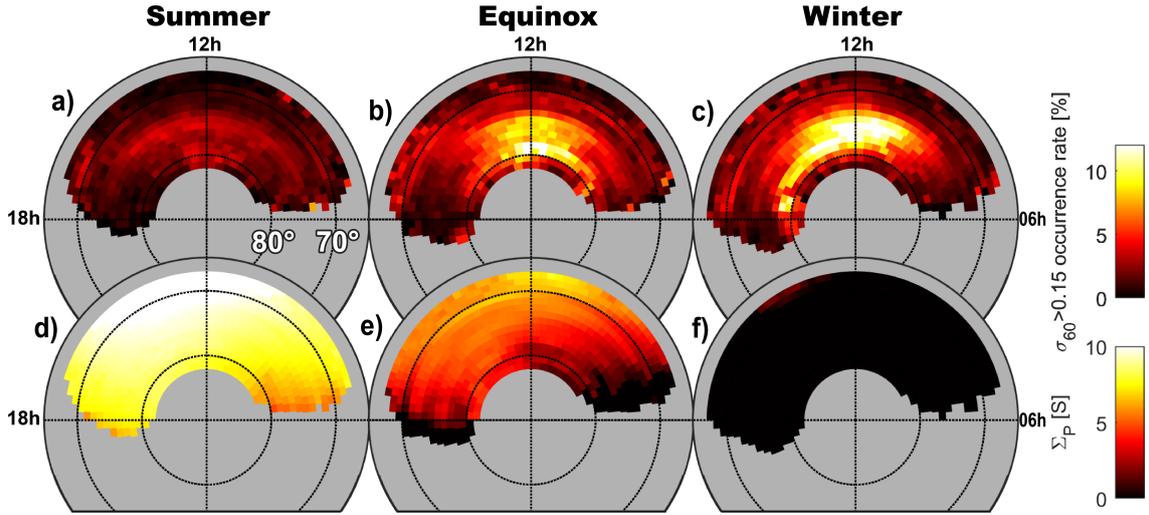
Figure 1. A dayside climatology for the years 2014-2016 of GNSS phase fluctuations (panels a-c), and a dayside climatology of Pedersen conductance induced by solar EUV photoionization (panels d-f), for the high-latitude (Magnetic Latitude, or MLAT, $> 68°$) northern hemisphere. Phase fluctuation events are recorded with ground-based receivers in Svalbard, Norway, and the occurrence of phase fluctuations are defined as the percentage of observations where the 60-second standard deviation of the detrended phase (σ_{60}) exceeds 0.15 radians. Conductance levels are calculated with an SZA-based model due to Moen and Brekke (1993), namely, $\Sigma_E = (F_{10.7})^{0.49} \left(0.34 \cos Z + 0.93 \cos^{1/2} Z \right)$. The data is aggregated in field-line-traced (altitude-corrected) geomagnetic coordinates (Baker and Wing, 1989), where magnetic noon is at the top and dusk to the right, and where we assume that the observed Pedersen conductance is located where Pedersen conductivity typically maximizes near 130–140 km (Kwak and Richmond, 2007). 'Summer' and 'winter' are calculated based on a 131-day window centered on the respective solstices, while 'Equinox' describes the rest of the data, dividing the calendar year into roughly three equal parts. Note the prominent "hot spot" of radio phase fluctuations near magnetic noon, which is caused by the magnetospheric cusp (see, e.g., Ivarsen et al., 2023). There are no major temporal gaps in the coverage of the GNSS data, and the observations provide a continous view of kilometer-scale gradients in the ionosphere above Svalbard.

Figure 1, we readily observe that whereas high-latitude conductance maximizes during local summer, the occurrence of plasma irregularities maximizes during local winter, with both quantities displaying a severe contrast between the two extrema.

The increased charge-carrier mobilities seen during summer and in aurorae effectively diffuse the kilometer-scale gradients associated with the phase fluctuations.

Another important reason for these strong, opposing trends is the ability of a conducting ionosphere to *short-circuit* the electric field that drives plasma instabilities (Vickrey and Kelley, 1982), where a highly conductive E-region allows Pedersen currents to close field-aligned currents, thereby neutralizing the perpendicular electric fields that would otherwise map to and drive instabilities in the F-region. The mechanism is well-studied and has been illuminated by, e.g., Kivanc and Heelis (1998), Ivarsen et al. (2019), and Ivarsen et al. (2021).

The above considerations substantiate the claim that the intermittent ionization caused by aurorae is of utmost importance for plasma dynamics in the dark, high-latitude ionosphere. In the absence of solar EUV ionization, particle precipitation is the main active source of ionization for the dark ionosphere, and the phenomenon has long been considered to cause both the growth and the decay of plasma irregularities, and the relationship between growth and decay is under debate (Ivarsen et al., 2024c).

To further elucidate the effects of increased conductance on the growth and decay of irregularities, we turn to an analysis of observations of precipitating particles, the routine source of ionization for the nightside auroral region of the ionosphere.

1.2 Precipitating particle ionization rate altitude profiles

We analyze a large database of precipitating particle observations from the instrument SSJ (Special Sensor J-series) (Redmon et al., 2017) onboard the many satellites belonging to the United States' Defense Meteorological Satellite Program (DMSP). The instrument provides an excellent estimation of the total precipitating particle flux (nominal range 30 eV–30 keV), though it misses certain broadband particles on account of its limited energy spectrum. We apply the fast parameterisations due to Fang et al. (2010) and Fang et al. (2013), and examine the average ionization rate altitude profiles that are characteristic to geomagnetic activity at various magnetic local times. In this paper, we ultimately discuss the inferred, or estimated, ratio of E-region (bottomside) to F-region (topside) conductance, and how this ratio should affect the many observations that have been made of plasma irregularities in the high-latitude ionosphere.

The conductivities depend on precipitating particles being stopped by the atmosphere, and they are being stopped in rates that are decided by the kinetic energy of the particles themselves, as well as the chemical composition of the atmospheric gas (air). The impacting particles ionize the gas, and so the density and molecular composition of the atmosphere lead to characteristic altitude-profiles of ionization rate. Notably, Fang et al. (2010) and Fang et al. (2013) presented parameterisations of time-consuming non-linear models of such ionization rate altitude profiles, enabling the fast calculation of millions of datapoints in aggregate.

Figure 2 shows an implementation of those equations to an example pair of precipitating electron and ion spectra, following the increased ionization rate in a natural path towards increased plasma density in the ionosphere, and consequent enhancements in *conductance*, the ability of the ionosphere to support electrical currents (Prölss, 2004a, b), culminating in the calculation of,

$$\eta \equiv \frac{\Sigma_E}{\Sigma_E + \Sigma_F}, \tag{1}$$

where $\Sigma_{E,F}$ represents Pedersen conductance (height-integrated Pedersen conductivity) in the E- and F-regions respectively (hereafter, 'conductance' refers to Pedersen conductance). Hall conductance affects Alfvén wave reflection (Ivarsen et al., 2020), we shall in this study restrict our scope to Pedersen conductance, as it is the primary agent for closing field-aligned currents and regulating cross-field diffusion in the Vickrey and Kelley (1982)-framework.

One may assume 170 km to be the boundary between those regions, a deliminator that follows the transition from O_2^+, NO^+-dominance to O^+-dominance in the ionosphere (Prölss, 2004a, b). While the profiles in Figure 2c–d) are useful, their

4
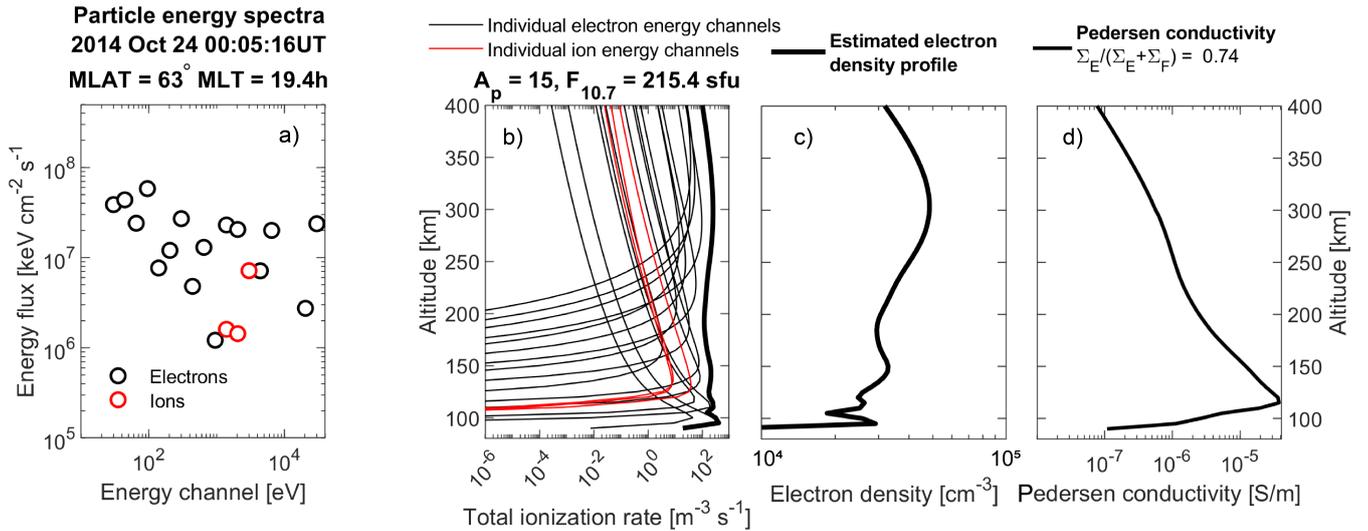
Figure 2. Panel a): a precipitating electron (black circles) and ion (red circles) spectrum observed by the DMSP F18 satellite on 24 October 2014. **Panel b):** the ionization rate altitude profiles based on the spectra, using the equations published by Fang et al. (2010) and Fang et al. (2013), together with the MSIS (Picone et al., 2002) model for the neutral atmosphere composition and the IGRF (Alken et al., 2021) model for magnetic field strengths. Solar and geomagnetic activity, for which the MSIS model is dependent, is indicated by the A_p- and $F_{10.7}$-indices. **Panel c):** Estimated plasma density profile, assuming that NO_+ dominates in the E-region, balancing production (ionization rate) with loss (recombination) (absent of solar EUV photoionization), under the assumption of a Chapman function above the F-peak. **Panel d):** Estimated conductivities resulting from particle collision interaction terms (Schunk and Nagy, 1980), using modelled compositions due to MSIS and IGRF. The ratio of E- to F-region conductance is indicated. See the supporting information for a more thorough description.

analysis must be accompanied by a clear admission of simplification by several assumptive steps (see Figure 2 caption and the Appendix A).

What follows is the presentation of three specialized analyses (Figures 3–5), each segmenting the estimated energy transfer from particle precipitation to ionization, segmented by spatial (geomagnetic coordinates) and temporal (geomagnetic activity) bins, and using data from the northern hemisphere winter, when overall conductivity is low. The efforts are not intending to present a general-statistical climatology, but are rather implemented to expose a characteristic behaviour of the high-latitude ionosphere, whose intrinsic implications demand our attention.

While the full energy cascade involved in the magnetosphere-ionosphere coupling is immensely complex, this study isolates one critical, measurable interaction within that coupling, which we iterate: the penetration depth of energetic particles systematically organising the ionospheric conductivity. The resulting conductance, in turn, acts as a crucial boundary condition that modulates the entire system, and its own collective response to all the external drivers. An isolated investigation into particle precipitation sheds light on a crucial mechanism that connect several plasma systems in geospace.
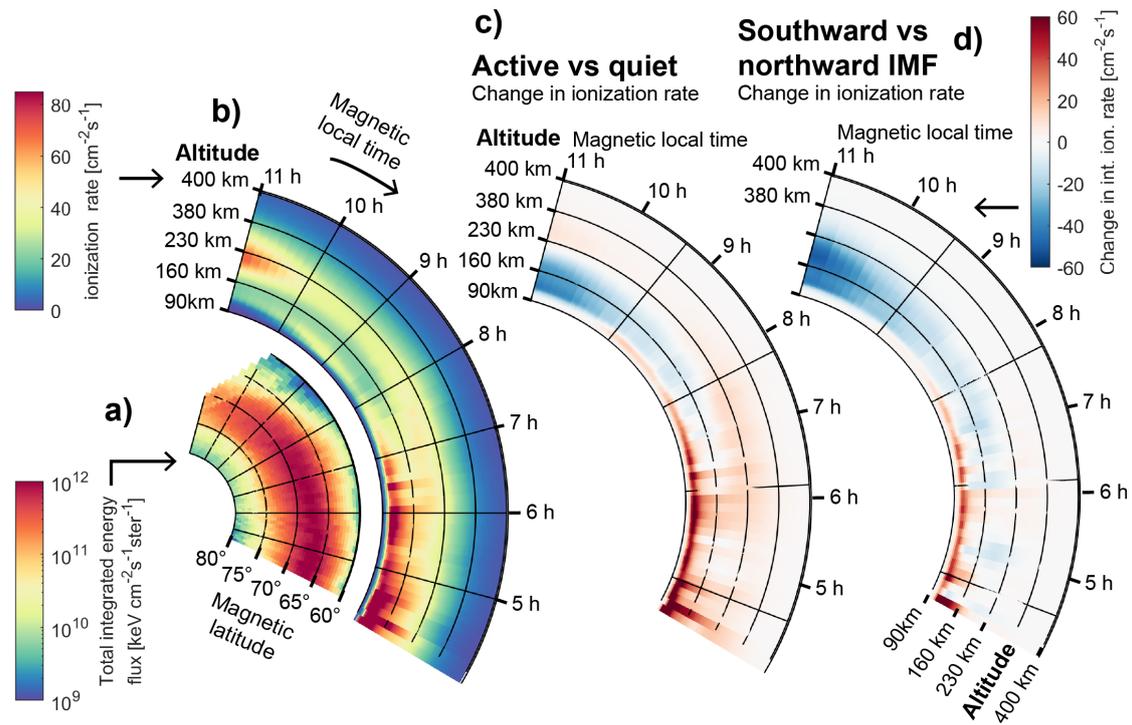
Figure 3. Panel a) shows total integrated energy flux of precipitating electrons and ions, binned by magnetic latitude (radial direction) and magnetic local time (azimuthal direction), based on 5 million precipitating particle spectra from the dawn-sector during northern hemisphere winter during the years 2014-2016, when the extent of solar EUV photoionization was minimal, using data gathered during geomagnetically active conditions (defined as measurement times when the auroral electrojet SME-index exceeded 150 nT). **Panel b)** shows the resulting altitude profiles (radial direction) of ionization rate, binned by magnetic local time (azimuthal direction). **Panels c) and d)** show ionization rate change, or contrast, defined as quiet subtracted from active (c) and southward subtracted from northward interplanetary magnetic field (IMF) configuration, based on bins of the data displayed in panel b). Note that 'southward and 'northward´ IMF configuration are defined as delineated by the bottom and top thirds of the ensemble while 'active´ and 'quiet´ are delineated by the median.

2   Some Trends

Figure 3 shows the first of the particular trends that we demonstrate in the present paper. We bin some 5 million precipitating particle spectra observed by all four DMSP satellites in the dawn- and pre-noon section of the northern hemisphere poleward of 60° magnetic latitude, collected during the local winter seasons of 2014–2016 (with winter defined as a 131-day period centered on the December solstice). In this region, spanning magnetic local times between 4h and 11h, the four satellites achieve excellent coverage, avoiding both the narrow gap centered around noon at lower latitudes and the wide gap centered on midnight. The figure reproduces a distinct and characteristic magnetic local time-trend that occurs during disturbed conditions (Newell et al., 2009, 2010; Ivarsen et al., 2024c). The well-known result confirms that the various and differing degree to which electrons precipitation defines the shape of the ionosphere's bottomside; with increased levels of particle precipitation,

the ionosphere *sags* towards midnight, where significant ionization (and free energy) is injected into the E-region. The result is a drastic decrease in the ratio of ionization experienced by the bottomside compared to the topside, as magnetic local time approaches noon.

125   The last two panels of Figure 3 estimate statistically how the above basic mechanism evolves in time, through changes in geomagnetic activity and interplanetary magnetic field configuration. Figure 3c) shows the altitude-dependent absolute changes in ionization rate implied by the DMSP-observed particle spectra, using a red-blue colorscale, where red indicates the excess ionization rate experienced during disturbed geomagnetic conditions, and where blue color indicates a *reduction* compared to geomagnetic quiet times (this time using the median value of 150 nT as deliminator). Figure 3d) presents the same comparison,

130   this time between southward and northward configurations of the interplanetary magnetic field (with red color indicating excess ionization during a southward field configuration). The results are likewise expected from comprehensive surveys (Newell et al., 2009, 2010) and studies that are narrowly focused on the cusp (Ivarsen et al., 2023), though we note the apparent and significant decrease in ionization rate at E-region altitudes around noon in Figures 3c–d), implying an absent electrical load for the field-lines in this region.

135   Together, the four panels of Figure 3 demonstrate that elevated levels of high-energy particle precipitation at dawn are accompanied by a decrease in such particle precipitation towards noon, causing a tilt (in magnetic local time) of the bottomside ionosphere during geomagnetic active times. Figure 4 explores this trend further, now showing altitude profiles for selected magnetic local times bins (a–e) as well as five geomagnetic activity bins in the noon-sector. The first row explores the tilting trend, accentuating how a general trend of a raised noon and lowered midnight are amplified during active times. In fact, for the

140   most extreme geomagnetic activity bin (top quintile in the SME-index), precipitation-induced ionization below 150 km (that are caused by electrons with energies up to 30 keV) is almost completely absent in the noon-sector.

     Next, we shall consider the tendency of the DMSP F18 satellite to consistently orbit through the noon-sector from the poleward-afternoon-side to the equatorward-morning-side of the cusp. This tendency is naturally exploited in a stretching & superposing orbital segment-scheme, comparing the median observations of ensembles of orbits. Figure 5a–c) detail some 352

145   conjunctions between the DMSP F18 satellite and ground-based GNSS receivers on Svalbard, Norway, during which the cusp was directly inferred in the data. Figure 5d–g) show two superposed orbit analyses, for both quiet and active conjunctions, where we compare the occurrence of GNSS phase fluctuations with observed ion drift speeds & the inferred ratio of E- to F-region conductance (Eq. 1).

     The stretched & superposed orbit analysis in Figure 5 reveals a clear, characteristic pattern in the inferred ratio of E- to F-

150   region conductance, η, where the poleward edge of the cusp marks the edge of a region in which E-region ionization is almost absent, leading to very low values of η (~ 0.25). On the other hand, the equatorward edge of the cusp marks the transition of a distinct high-η region (> 0.7): this is the characteristic diffuse aurora that we typically find equatorward of the cusp (Newell et al., 2010; Ivarsen et al., 2024c, 2025d).

     Whereas we are unable to capture the entire ionosphere-magnetosphere-thermosphere energy transfer in the relatively iso-

155   lated dataset of precipitating particles, this analysis does demonstrate a systematic variation in penetration depth of precipitating particles, an important quantity that is important by merit of its interconnectedness in geospace. A comparative analysis of the
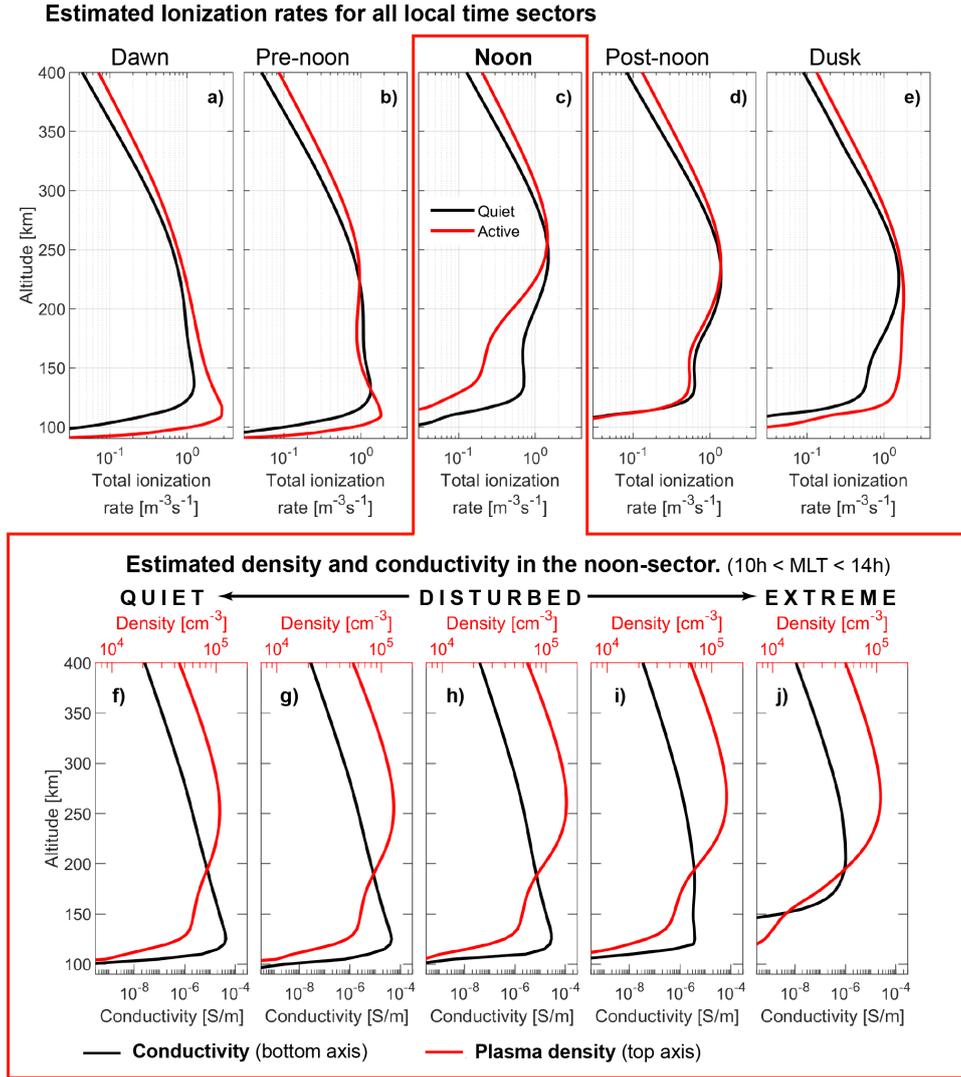
Figure 4. Ionization rate **(panels a–e)** and density & conductivity **(f–j)** profiles, for bins in magnetic local time **(a–e)** and geomagnetic activity **(f–j)**, where the latter five panels show data only from the *noon-sector*. We define the sectors dawn (03-07 MLT), pre-noon (07-11 MLT), noon (11-13 MLT), post-noon (13-17 MLT), and dusk (17-21 MLT). In **panels a–e)**, black and red curve correspond to quiet and active geomagnetic activity level respectively (the upper and lower third in the SME-index distribution, around 70 nT and 150 nT respectively), while in **panels f–j)**, black and red curve denote conductivity and plasma density, respectively. Curves denote median, omitting a considerable variation within the aggregate. The analysis is based on 5 million measurement points made during northern hemisphere winter during the years 2014-2016.
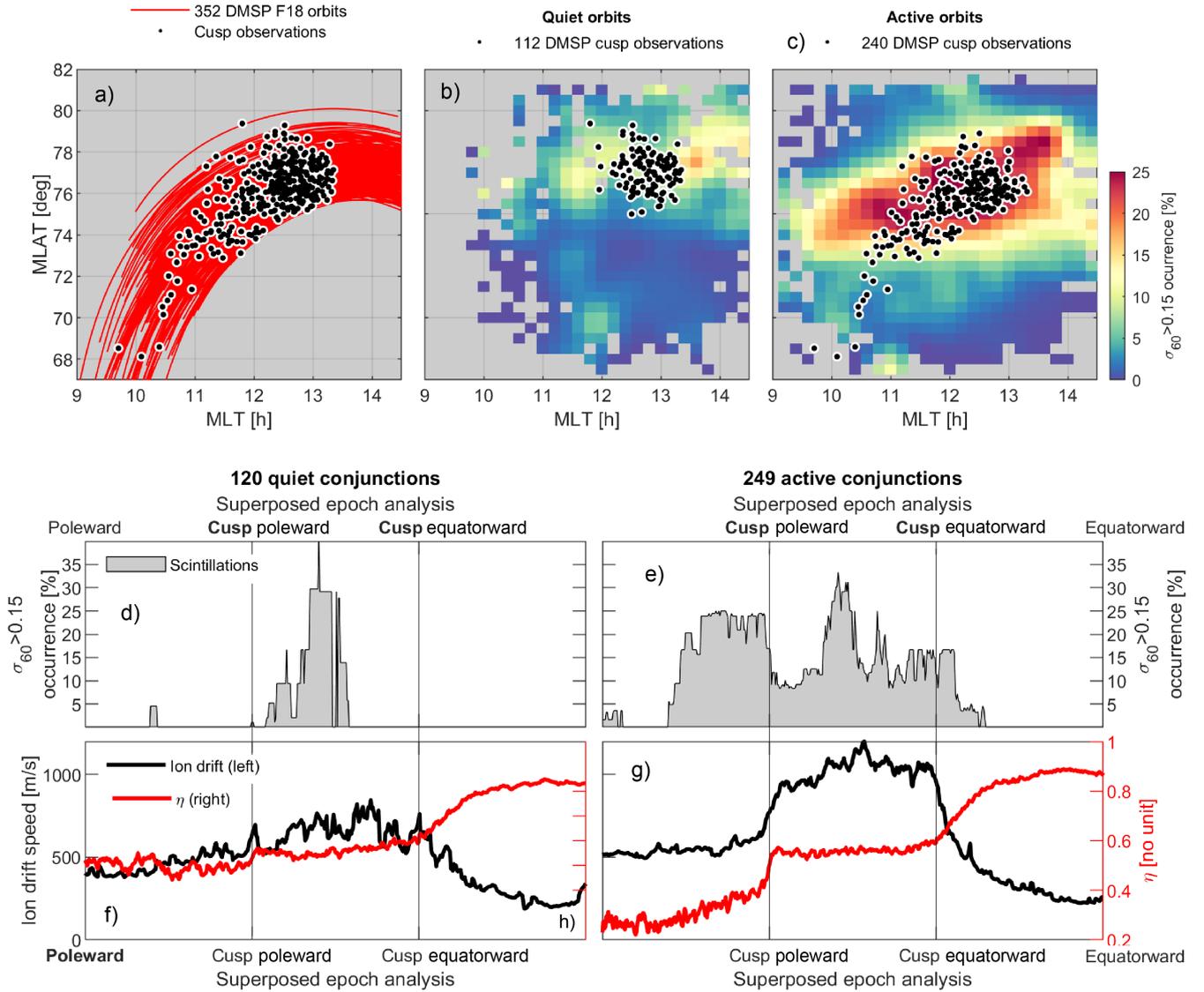
Figure 5. 352 northern hemisphere winter conjunctions between the DMSP F18 satellite and the distributed pierce points implied by three ground-based GNSS receivers, mapped assuming an IPP altitude of 350 km, consistent with F-region irregularities (Madhanakumar et al., 2024). We show orbits where the cusp was identified according to the definitions due to Newell and Meng (1988) in **(panel a)**. These conjunctions are divided into relatively quiet- (SME < 135 nT, **panel b**) and active-time (SME > 135 nT, **panel c**) aggregates, superposed on the spatial occurrence rate of phase fluctuation events in the surrounding region. In **panels d–e)** the occurrence rate of phase fluctuations in the region is shown for the quiet (d) and active (e) conjunctions, now in a stretched & superposed orbit analysis, with the poleward and equatorward edges of the cusp stretched to match across the superposed orbits. An equal portion of each orbit is used for the three segments. **Panels f–g)** show the same stretched & superposed orbit analysis, this time displaying the cross-track ion drift speeds observed during the orbits (black) and η, the ratio of E- to F-region conductance (Eq. 1).

simultaneously observed occurrence rates of radio phase fluctuations ties the dramatic spatial gradient in η to the occurrence rate of ionospheric structuring in general. The next section will present a discussion of the *consequences* of these gradients in the ionospheric boundary condition, for the purpose of ionosphere-magnetosphere coupling and current closure, and of influencing when and where plasma instabilities can grow or are suppressed.

3   Discussion

Comparing Figure 5e) and Figure 5g) we observe that the low-η region poleward of the cusp is accompanied by elevated occurrence rates of phase fluctuations. This action is caused by the proliferation of polar cap patches (Jin et al., 2014), drifting poleward from the cusp, for example created by a tongue-of-ionization action (Hosokawa et al., 2010b) or seeded by poleward-moving auroral forms (Frey et al., 2019). The growth of turbulence on the edges of these patches are no doubt aided by low values of η, which should suppress the ability of the E-region to short-circuit the electric fields that sustain F-region plasma instabilities (Vickrey and Kelley, 1982; Ivarsen et al., 2021, 2024c).

Adding to this picture are the ion drift observations shown in Figure 5f–g). These drifts, driven by strong convection electric fields (and the process of dayside reconnection), represent the primary source of free energy that can generate F-region irregularities in the region. Notably, the drift speeds are highest not poleward or equatorward of the cusp, but directly *inside it*, peaking where the conductance ratio η is transitioning from low to high values. This allows us to view the cusp as an "instability factory": it is the region that combines the strongest driver (electric fields; see, e.g., Tsunoda, 1988) with a relatively weak inhibitor (decreasing η values). The irregularities generated here then convect poleward into a region where, although the drift speed is lower, the inhibitor is almost nonexistent (η is at its lowest). This allows the turbulence that occurs during local winter to persist for long periods as it populates the polar cap (Wood and Pryse, 2010; Ivarsen et al., 2021; Eriksen et al., 2023). Consistent with the η-paradigm, occurrences of the "tongue of ionization", a large, continuous blob of ionization that stretches from the cusp and into the polar cap (Foster et al., 2005) are likewise associated with radio phase fluctuations (De Franceschi et al., 2008; van der Meeren et al., 2014). Conversely, equatorward of the cusp, both the driver (drift speed) and the turbulence itself are suppressed, both short-circuited by drastic increases in conductance (Figures 3–4). This dynamic interplay between the convection driver and the E-region conductance inhibitor is entirely consistent with established observations and inferences of the irregularity landscape poleward of the cusp (Jin et al., 2017; Eriksen et al., 2023; Madhanakumar et al., 2024).

A key aspect of the prevailing picture is the decrease, or even collapse, in energetic particle precipitation inside the noon-sector. It would then seem that the energetic particle precipitation from the radiation belts that normally sustain the dark, dayside E-region (Spasojevic and Inan, 2010; Nishimura et al., 2013; Ni et al., 2014) are effectively drained out from the cusp-region, consistent with recent observations (Ivarsen et al., 2023). This draining is taken to account for the energy budget there being largely dominated by dayside magnetic reconnection, and parts of this energy expenditure will occur through broadband particle precipitation that is missed by the DMSP instrumentation, which is more efficient at probing intense high-energy diffuse aurorae. The mentioned collapse in high-energy electron precipitation is therefore marking the *change in energy input from unstable wave energy on closed magnetic field-lines to a wave energy cascade controlled by magnetic reconnection.*

We emphasize that this study focuses on the dark winter ionosphere where solar EUV conductance is negligible, an so, While the dayside cusp is pushed by Alfvénic Poynting flux (see, e.g., Chaston et al., 2007) and soft particle precipitation, the specific lack of high-energy precipitation results in a 'hollow' conductivity profile (low η) distinct from the auroral oval.

Indeed, Figure 4 shows that while the E-region at noon collapses, the E-region at dawn and dusk is significantly enhanced during active times, and especially so for the dawn sector. This reflects the substorm cycle, in which energetic particles injected near midnight drift around Earth, eastward towards dawn (Kamide and Kokubun, 1996), providing a robust source of hot electrons that precipitate owing to pitch-angle scattering (Thorne et al., 2010), evident as the eastward "sagging" of the ionosphere in Figure 4.

At our onset, Figure 1 illustrated a well-known fact, namely that lower conductivities in the ionosphere is generally associated with an increase in the detrimental effects caused by high-latitude plasma turbulence, capturing a rather small part of the entire energy cascade from large, unstable wave modes in the magnetosphere. Figures 3 and 4 then recreated several known trends in the penetration heights of particle precipitation. Building on these established results, we described the spatial gradient in η and how it affects electrodynamics. Figure 5 applied a stretching & superposing orbit analysis to examine a prominent transition zone in η, the ionospheric cusp, showing a statistically clear relation between η and the occurrence rates of phase fluctuations, in accordance with expectations based on η as a crucial regulator of the effective growth rates of F-region instabilities. The results of this analysis demonstrated the explanatory value of examining boundary conditions in η as regulators of plasma instabilities in the ionosphere.

The regulation of turbulence by conductivity is not merely a passive damping process. Strong conductivity gradients, such as those found at the edges of auroral forms, necessitate the formation of polarization electric fields to maintain current continuity (the Cowling effect, Fujii et al., 2011). These electrostatic realities can locally drive plasma drifts, effectively sustaining the turbulence initially triggered by magnetospheric inputs.

On that note, though, we point out that several important chemical and electrodynamic factors are broadly simplified in the present paper, and we isolate a narrow component of a large and complicated energy cascade. Our statistical application of the (Fang et al., 2010, 2013)-equations is likewise simplified in terms of *chemistry* (see Appendix A). Furthermore, we note that DMSP spectra do not fully capture particles below 30 eV. However, such soft precipitation, typical of the cusp (Newell et al., 2009), would primarily ionize the F-region, further lowering the η ratio and reinforcing the contrast with the E-region-dominated auroral oval. Our results are therefore conservative with respect to the real magnitude of the η contrast.

At any rate, our albeit interesting results must be interpreted with caution, and more thorough investigations of their validity and ramification must follow. Here, we recommend the use of extensive magnetosphere-ionosphere coupling models that aim to capture the energy cascade, taking kinetic processes into account (Wiltberger et al., 2017).

4 Conclusions

We have applied fast parameterisations of ionization rate altitude profiles due to Fang et al. (2010) and Fang et al. (2013) to a large database of precipitating particle observations from the high-latitude, northern hemisphere ionosphere, observed during

local winter. The efforts have yielded several characteristic trends in the altitude-dependent ionization rate, distinguishing between magnetic local times and various levels of geomagnetic activity. While the calculations at times are based on a wide array of simplifications (the characteristic development in η on display in Figure 5, for example), the trends uncovered are clear and convincing.

To see how these trends intersect with the current understanding of the greater energy- and momentum transfer that dominates geospace, we offer the following thoughts. The interconnected plasma environment as a whole is in a steady state MHD flow at all times. Excursions *away* from that equilibrium, in this case observations of particle precipitation, reflect an ongoing cascade of unstable wave energy from larger (ultra-low frequency) to smaller (kinetic) scales, a cascade whose purpose is to *restore equilibrium* through heat expenditure. Certain unstable modes interact in what are essentially complex and manifold ways to produce the observed proliferation of small-scale structuring in the auroral ionosphere's plasma, whether through kinetic Alfvén waves or wave-particle interactions.

The object of the present study, a database of particle precipitation observations, despite the deficiency in essentially being a dataset in isolate, contain a direct path for energetic particle precipitation to affect the triggering of F-region instabilities, and thereby regulate the occurrences of irregularities in the ionosphere plasma. We have arrived at our results through simplified calculations of ionization altitude and the physics of ambipolar diffusion in the kinetic plasma that forms on the boundary of Earth's dense atmosphere.

Prohibitively fast ambipolar diffusion caused by high conductance is efficient at smoothing out gradients at all scales (Moisan and Pelletier, 2012). Recent demonstrations of the direct and largely instantaneous signal retention by the turbulent E-region (Shen et al., 2024; Ivarsen et al., 2024a, b, 2025a, c) are consistent with the origin of the signal being a structural imprint of magnetospheric wave processes, a pattern that dissipates through non-linear heating of the plasma (St-Maurice and Goodwin, 2021). The very ephemeral quality of the turbulent processes (they die out very fast) points to the presence of fast, efficient dissipation enabled by enhancements in conductance.

The present study provides an exposition of the negating effect that high conductivities can have for instability growth in the F-region ionosphere, where an electrodynamic description of the ionosphere at impact isolate the influence that conductance demands over ambipolar diffusion in a plasma rich in ion-neutral collisions (roughly 90 km – 150 km altitude). We show that when ionization sources cease and conductance is nominally low and decreasing, the structuring of F-region plasma responds in predictable ways, increasing in occurrence and magnitude.

We have reached these results through a simple statistical analysis of a large dataset, and further experiments are necessary to understand the plasma physics involved with damping (La Rosa and Hysell, 2025), and the effects of non-linear conductivity on geospace as a whole (Wiltberger et al., 2017).

Appendix A: Some details on the Method

260 We use a database of precipitating electron data from the SSJ instrument on the F16, F17, F18, and F19 satellites of the DMSP. The DMSP satellites are in helio-synchronous dawn-dusk 800 km-altitude polar orbits covering most of the dayside high-latitude ionosphere in the northern hemisphere. The SSJ instrument uses particle detectors to measure the energy flux of precipitating electrons and ions through 19 energy channels from 30 eV to 30 keV, with a cadence of 1 second Redmon et al. (2017). The DMSP satellites' orbits cover the high-latitude northern hemisphere dayside, with no coverage in the midnight
265 sector between 21h and 3h.

Example precipitating particle spectra are presented in Figure 2a, and what follows is a detailed explanation of the steps that lead to Figure 2b–d.

A1   From Particle Spectra to Ionization Rate

Each of the 19 energy channels from the DMSP SSJ instrument is treated as a monoenergetic beam, and the resulting ionization
270 rate profiles that are obtained by an implementation of Fang et al. (2010) and Fang et al. (2013) are summed to get the total profile shown in Figure 2b. The state of the neutral atmosphere is captured by the A_P- and $F_{10.7}$-indices, and we use average, pre-calculated model atmospheres based on representative solar local times and latitudes.

A2   From Ionization Rate to Electron Density

Under conditions of darkness (no solar EUV photoionization), the steady-state electron density n_e in the E-region is determined
275 by the balance between production (ionization rate) and loss (recombination), and we assume that NO_+ dominates in the E-region. That gives a plasma density equal to the square root of the ionization rate divided by the recombination rate of NO_+ (Prölss, 2004a, b),

$$n_e = \sqrt{\frac{q}{\alpha}}, \tag{A1}$$

with q being ionization rate, α being recombination rate, and n_e plasma density. We use values for α from Sheehan and St.-
280 Maurice (2004). This gives a density profile in the E-region and lower F-region. From the F-peak, we apply the Chapman-α equation upwards, using ionized gas scale heights from an empirical model due to Li et al. (2019).

A3   From Electron Density to Pedersen Conductivity

Based on the estimated plasma density profile, we exploit expressions for ion-neutral and neutral-neutral collision rates to estimate Pedersen conductivity, following Ivarsen et al. (2021). In short, we use expressions for collision interaction terms

between all charged particles associated with the ion species in the ionosphere, as presented in Schunk and Nagy (1980). Then, we use the International Reference Ionosphere model (IRI) for the ionospheric ion species *proportions* (Bilitza et al., 2022), using the DMSP-estimated plasma density to determine species densities. IRI also provides electron temperature, we use MSIS for the neutral number densities, and IGRF for the magnetic field strength (Thébault et al., 2015). Although the many models doubtless influence the final density and conductivity values greatly, the main source of variability in our result stem from variability in the precipitating energy flux.

Pedersen conductivity is then arrived at via,

$$\sigma_P = \frac{n_e e^2}{m_i}\left(\frac{\nu_{in}}{\nu_{in}^2 + \Omega_i^2}\right) + \frac{n_e e^2}{m_e}\left(\frac{\nu_{en}}{\nu_{en}^2 + \Omega_e^2}\right), \tag{A2}$$

where σ_P is the Pedersen conductivity, e is the elementary charge, $m_{i,e}$ are the ion and electron masses, respectively, $\nu_{in,en}$ are the ion-neutral and electron-neutral collision frequencies, respectively, and $\Omega_{i,e}$ are the ion and electron gyrofrequencies, respectively. We then calculate the conductances that enter into Eq. (1), by integrating Pedersen conductivity in the E- and F-regions,

$$\Sigma_{\text{E,F}} = \int_{\text{E,F}} \sigma(h)\, dh. \tag{A3}$$

E-region conductance is dominated by ionization at the nominal Pedersen conductivity peak, which we take as near 130–140 km, with falling conductivity towards 170 km (Kwak and Richmond, 2007). The transition height between the E- and F-region differ, and we conservatively take 170 km to be the boundary, which roughly matches the transition from O_2^+, NO^+-dominance to O^+-dominance Prölss (2004a, b).

A4 The Compounding Effect of Thermospheric Neutral Density

The MSIS model, upon whose foundation the Fang et al. (2010) and Fang et al. (2013) parametrizations are implemented in the present paper, accounts for the atmospheric expansion during geomagnetic storms. This important notion, that the thermosphere heats up and expands during storms in geospace, can be quantified.
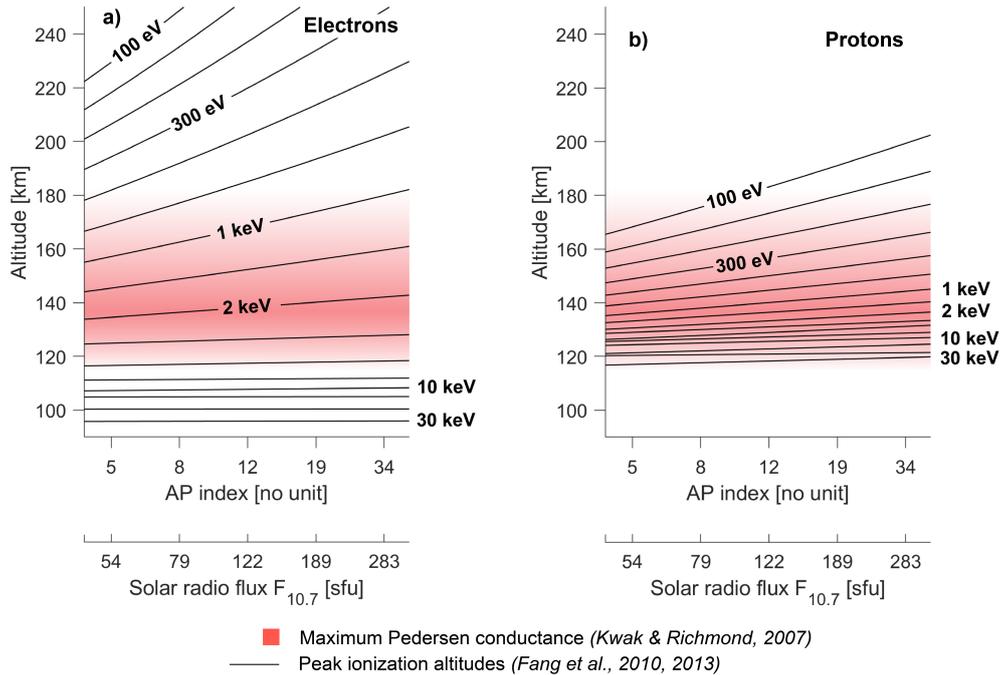
This physical process works in concert with the changing particle spectra: for any given energy, a particle will be stopped at a higher altitude, owing to increased densities at higher altitudes. This "swelling" of the atmosphere would, by itself, tend to raise the ionization profile and slightly *decrease* the η conductance ratio. This effect likely complements the much more dramatic effect of the spectral changes, and contributes to a deeper, more nuanced understanding of the coupled system.

Figure A1 quantifies the effect, by keeping precipitating particle spectra uniform and constant, varying only the A_P- and $F_{10.7}$-indices. In critical situations, say, cases of extreme thermospheric swelling, the effect may influence the closing of magnetospheric current systems and the charge-carrier mobility that supports such currents. The topic should be investigated further, in future holistic models of the coupled atmosphere-ionosphere-magnetosphere system.

Figure A1. Peak ionization altitudes for uniform monoenergetic electrons (a) and protons (b) for 120 MSIS-based model atmospheres. The y-axis shows altitude and the x-axis shows the AP-index and $F_{10.7}$ solar radio flux values upon which the model atmospheres are based. Each black line represents the peak altitude for particles with energies ranging from 100 eV to 30 keV, while red shaded regions indicate the altitude range at which Pedersen conductance normally maximizes, from Kwak and Richmond (2007).

15

References

Alken, P., Thébault, E., Beggan, C. D., Amit, H., Aubert, J., Baerenzung, J., Bondar, T. N., Brown, W. J., Califf, S., Chambodut, A., Chulliat, A., Cox, G. A., Finlay, C. C., Fournier, A., Gillet, N., Grayver, A., Hammer, M. D., Holschneider, M., Huder, L., Hulot, G., Jager, T., Kloss, C., Korte, M., Kuang, W., Kuvshinov, A., Langlais, B., Léger, J.-M., Lesur, V., Livermore, P. W., Lowes, F. J., Macmillan, S., Magnes, W., Mandea, M., Marsal, S., Matzka, J., Metman, M. C., Minami, T., Morschhauser, A., Mound, J. E., Nair, M., Nakano, S., Olsen, N., Pavón-Carrasco, F. J., Petrov, V. G., Ropp, G., Rother, M., Sabaka, T. J., Sanchez, S., Saturnino, D., Schnepf, N. R., Shen, X., Stolle, C., Tangborn, A., Tøffner-Clausen, L., Toh, H., Torta, J. M., Varner, J., Vervelidou, F., Vigneron, P., Wardinski, I., Wicht, J., Woods, A., Yang, Y., Zeren, Z., and Zhou, B.: International Geomagnetic Reference Field: The Thirteenth Generation, Earth, Planets and Space, 73, 49, https://doi.org/10.1186/s40623-020-01288-x, 2021.

Baker, K. B. and Wing, S.: A New Magnetic Coordinate System for Conjugate Studies at High Latitudes, Journal of Geophysical Research: Space Physics, 94, 9139–9143, https://doi.org/10.1029/JA094iA07p09139, 1989.

Bilitza, D., Pezzopane, M., Truhlik, V., Altadill, D., Reinisch, B. W., and Pignalberi, A.: The International Reference Ionosphere Model: A Review and Description of an Ionospheric Benchmark, Reviews of Geophysics, 60, e2022RG000 792, https://doi.org/10.1029/2022RG000792, 2022.

Borovsky, J. E.: Looking for Evidence of Mixing in the Solar Wind from 0.31 to 0.98 AU, Journal of Geophysical Research: Space Physics, 117, https://doi.org/10.1029/2012JA017525, 2012.

Borovsky, J. E., Birn, J., Echim, M. M., Fujita, S., Lysak, R. L., Knudsen, D. J., Marghitu, O., Otto, A., Watanabe, T.-H., and Tanaka, T.: Quiescent Discrete Auroral Arcs: A Review of Magnetospheric Generator Mechanisms, Space Science Reviews, 216, 1, https://doi.org/10.1007/s11214-019-0619-5, 2019.

Chaston, C. C., Carlson, C. W., McFadden, J. P., Ergun, R. E., and Strangeway, R. J.: How Important Are Dispersive Alfvén Waves for Auroral Particle Acceleration?, Geophysical Research Letters, 34, https://doi.org/10.1029/2006GL029144, 2007.

Conroy, J. P., Deshpande, K., Scales, W., and Zaghloul, A.: Statistical Analysis of Refractive and Diffractive Scintillation at High Latitudes, Radio Science, 57, e2021RS007 259, https://doi.org/10.1029/2021RS007259, 2022.

Cowley, S. W. H.: TUTORIAL: Magnetosphere-Ionosphere Interactions: A Tutorial Review, Washington DC American Geophysical Union Geophysical Monograph Series, 118, 91, https://doi.org/10.1029/GM118p0091, 2000.

David, V. and Galtier, S.: K_\perp ^-8/3 Spectrum in Kinetic Alfvén Wave Turbulence: Implications for the Solar Wind, The Astrophysical Journal Letters, 880, L10, https://doi.org/10.3847/2041-8213/ab2fe6, 2019.

De Franceschi, G., Alfonsi, L., Romano, V., Aquino, M., Dodson, A., Mitchell, C. N., Spencer, P., and Wernik, A. W.: Dynamics of High-Latitude Patches and Associated Small-Scale Irregularities during the October and November 2003 Storms, Journal of Atmospheric and Solar-Terrestrial Physics, 70, 879–888, https://doi.org/10.1016/j.jastp.2007.05.018, 2008.

Dimant, Y. S., Khazanov, G. V., and Oppenheim, M. M.: Effects of Electron Precipitation on E-Region Instabilities: Theoretical Analysis, Journal of Geophysical Research: Space Physics, 126, e2021JA029 884, https://doi.org/10.1029/2021JA029884, 2021.

Eriksen, N. K., Lorentzen, D. A., Oksavik, K., Baddeley, L., Hosokawa, K., Shiokawa, K., Bland, E., Paxton, L., Zhang, Y., McWilliams, K., Yeoman, T., and Themens, D. R.: On the Creation, Depletion, and End of Life of Polar Cap Patches, Journal of Geophysical Research: Space Physics, 128, e2023JA031 739, https://doi.org/10.1029/2023JA031739, 2023.

Fang, X., Randall, C. E., Lummerzheim, D., Wang, W., Lu, G., Solomon, S. C., and Frahm, R. A.: Parameterization of Monoenergetic Electron Impact Ionization, Geophysical Research Letters, 37, https://doi.org/10.1029/2010GL045406, 2010.

355   Fang, X., Lummerzheim, D., and Jackman, C. H.: Proton Impact Ionization and a Fast Calculation Method, Journal of Geophysical Research: Space Physics, 118, 5369–5378, https://doi.org/10.1002/jgra.50484, 2013.

Foster, J. C., Coster, A. J., Erickson, P. J., Holt, J. M., Lind, F. D., Rideout, W., McCready, M., van Eyken, A., Barnes, R. J., Greenwald, R. A., and Rich, F. J.: Multiradar Observations of the Polar Tongue of Ionization, Journal of Geophysical Research: Space Physics, 110, https://doi.org/10.1029/2004JA010928, 2005.

360   Frey, H. U., Han, D., Kataoka, R., Lessard, M. R., Milan, S. E., Nishimura, Y., Strangeway, R. J., and Zou, Y.: Dayside Aurora, Space Science Reviews, 215, 51, https://doi.org/10.1007/s11214-019-0617-7, 2019.

Fujii, R., Amm, O., Yoshikawa, A., Ieda, A., and Vanhamäki, H.: Reformulation and Energy Flow of the Cowling Channel, Journal of Geophysical Research: Space Physics, 116, https://doi.org/10.1029/2010JA015989, 2011.

Ghobadi, H., Spogli, L., Alfonsi, L., Cesaroni, C., Cicone, A., Linty, N., Romano, V., and Cafaro, M.: Disentangling Iono-
365   spheric Refraction and Diffraction Effects in GNSS Raw Phase through Fast Iterative Filtering Technique, GPS Solutions, 24, 85, https://doi.org/10.1007/s10291-020-01001-1, 2020.

Greene, K., Miles, D. M., Bounds, S. R., Bonnell, J. W., Feltman, C., Roglans, R., and Streltsov, A.: In Situ Evidence of Ionospheric Feedback Instability Adjacent to a Quiescent Auroral Arc, Geophysical Research Letters, 52, e2024GL110479, https://doi.org/10.1029/2024GL110479, 2025.

370   Hosokawa, K., Kadokura, A., Sato, N., Milan, S. E., Lester, M., Bjornsson, G., and Saemundsson, Th.: Electric Field Modulation behind Pulsating Aurora, Journal of Geophysical Research: Space Physics, 113, https://doi.org/10.1029/2008JA013601, 2008.

Hosokawa, K., Ogawa, Y., Kadokura, A., Miyaoka, H., and Sato, N.: Modulation of Ionospheric Conductance and Electric Field Associated with Pulsating Aurora, Journal of Geophysical Research: Space Physics, 115, https://doi.org/10.1029/2009JA014683, 2010a.

Hosokawa, K., Tsugawa, T., Shiokawa, K., Otsuka, Y., Nishitani, N., Ogawa, T., and Hairston, M. R.: Dynamic Temporal Evo-
375   lution of Polar Cap Tongue of Ionization during Magnetic Storm, Journal of Geophysical Research: Space Physics, 115, https://doi.org/10.1029/2010JA015848, 2010b.

Huba, J. D., Hassam, A. B., Schwartz, I. B., and Keskinen, M. J.: Ionospheric Turbulence: Interchange Instabilities and Chaotic Fluid Behavior, Geophysical Research Letters, 12, 65–68, https://doi.org/10.1029/GL012i001p00065, 1985.

Ivarsen, M. F., Jin, Y., Spicher, A., and Clausen, L. B. N.: Direct Evidence for the Dissipation of Small-Scale Ionospheric Plasma Structures
380   by a Conductive E Region, Journal of Geophysical Research: Space Physics, 124, 2935–2942, https://doi.org/10.1029/2019JA026500, 2019.

Ivarsen, M. F., Park, J., Kwak, Y.-S., Jin, Y., Knudsen, D. J., and Clausen, L. B. N.: Observational Evidence for the Role of Hall Conductance in Alfvén Wave Reflection, Journal of Geophysical Research: Space Physics, 125, e2020JA028119, https://doi.org/10.1029/2020JA028119, 2020.

385   Ivarsen, M. F., Jin, Y., Spicher, A., Miloch, W., and Clausen, L. B. N.: The Lifetimes of Plasma Structures at High Latitudes, Journal of Geophysical Research: Space Physics, 126, e2020JA028117, https://doi.org/10.1029/2020JA028117, 2021.

Ivarsen, M. F., Jin, Y., Spicher, A., St-Maurice, J.-P., Park, J., and Billett, D.: GNSS Scintillations in the Cusp, and the Role of Precipitating Particle Energy Fluxes, Journal of Geophysical Research: Space Physics, 128, e2023JA031849, https://doi.org/10.1029/2023JA031849, 2023.

390   Ivarsen, M. F., Gillies, M. D., Huyghebaert, D. R., St-Maurice, J.-P., Lozinsky, A., Galeschuk, D., Donovan, E., and Hussey, G. C.: Turbulence Embedded Into the Ionosphere by Electromagnetic Waves, Journal of Geophysical Research: Space Physics, 129, e2023JA032310, https://doi.org/10.1029/2023JA032310, 2024a.

Ivarsen, M. F., St-Maurice, J.-P., Huyghebaert, D. R., Gillies, M. D., Lind, F., Pitzel, B., and Hussey, G. C.: Deriving the Ionospheric Electric Field From the Bulk Motion of Radar Aurora in the E-Region, Journal of Geophysical Research: Space Physics, 129, e2024JA033 060, https://doi.org/10.1029/2024JA033060, 2024b.

Ivarsen, M. F., St-Maurice, J.-P., Jin, Y., Park, J., Buschman, L. M., and Clausen, L. B.: To What Degree Does the High-Energy Aurora Destroy F-region Irregularities?, Frontiers in Astronomy and Space Sciences, 11, https://doi.org/10.3389/fspas.2024.1309136, 2024c.

Ivarsen, M. F., Miyashita, Y., St-Maurice, J.-P., Hussey, G. C., Pitzel, B., Galeschuk, D., Marei, S., Horne, R. B., Kasahara, Y., Matsuda, S., Kasahara, S., Keika, K., Miyoshi, Y., Yamamoto, K., Shinbori, A., Huyghebaert, D. R., Matsuoka, A., Yokota, S., and Tsuchiya, F.: Characteristic E-Region Plasma Signature of Magnetospheric Wave-Particle Interactions, Physical Review Letters, 134, 145 201, https://doi.org/10.1103/PhysRevLett.134.145201, 2025a.

Ivarsen, M. F., Song, K., Spogli, L., St-Maurice, J.-P., Pitzel, B., Marei, S., Huyghebaert, D. R., Kasahara, S., Keika, K., Miyoshi, Y., Hori, T., Themens, D. R., Kazama, Y., Wang, S.-Y., Matsuoka, A., Shinohara, I., Mitani, T., Yokota, S., Jayachandran, P. T., and Hussey, G. C.: Direct Forcing of the Collisional Auroral Ionosphere by Kinetic Alfvén Turbulence, https://doi.org/10.48550/arXiv.2507.11755, 2025b.

Ivarsen, M. F., St-Maurice, J.-P., Hussey, G. C., Billet, D., Huyghebaert, D. R., Jin, Y., Miyashita, Y., Kasahara, S., Song, K., Jayachandran, P. T., Yokota, S., Miyoshi, Y., Yamamoto, K., Shinbori, A., Kasahara, Y., Shinohara, I., and Matsuoka, A.: Eastward Transients in the Dayside Ionosphere. I. Electrodynamics on Closed Field Lines, Physical Review E, 112, 045 204, https://doi.org/10.1103/r6bv-pzlq, 2025c.

Ivarsen, M. F., St-Maurice, J.-P., Hussey, G. C., McWilliams, K., Jin, Y., Huyghebaert, D. R., Miyashita, Y., and Sibeck, D.: Eastward Transients in the Dayside Ionosphere. II. A Parallel-Plate Capacitorlike Effect, Physical Review E, 112, 045 203, https://doi.org/10.1103/3bzj-bsf8, 2025d.

Jin, Y., Moen, J. I., and Miloch, W. J.: GPS Scintillation Effects Associated with Polar Cap Patches and Substorm Auroral Activity: Direct Comparison, Journal of Space Weather and Space Climate, 4, A23, https://doi.org/10.1051/swsc/2014019, 2014.

Jin, Y., Moen, J. I., Oksavik, K., Spicher, A., Clausen, L. B. N., and Miloch, W. J.: GPS Scintillations Associated with Cusp Dynamics and Polar Cap Patches, Journal of Space Weather and Space Climate, 7, A23, https://doi.org/10.1051/swsc/2017022, 2017.

Kamide, Y. and Kokubun, S.: Two-Component Auroral Electrojet: Importance for Substorm Studies, Journal of Geophysical Research: Space Physics, 101, 13 027–13 046, https://doi.org/10.1029/96JA00142, 1996.

Kasahara, Y., Kasaba, Y., Kojima, H., Yagitani, S., Ishisaka, K., Kumamoto, A., Tsuchiya, F., Ozaki, M., Matsuda, S., Imachi, T., Miyoshi, Y., Hikishima, M., Katoh, Y., Ota, M., Shoji, M., Matsuoka, A., and Shinohara, I.: The Plasma Wave Experiment (PWE) on Board the Arase (ERG) Satellite, Earth, Planets and Space, 70, 86, https://doi.org/10.1186/s40623-018-0842-4, 2018.

Keiling, A., Wygant, J. R., Cattell, C. A., Mozer, F. S., and Russell, C. T.: The Global Morphology of Wave Poynting Flux: Powering the Aurora, Science, 299, 383–386, https://doi.org/10.1126/science.1080073, 2003.

Keskinen, M. J. and Huba, J. D.: Nonlinear Evolution of High-Latitude Ionospheric Interchange Instabilities with Scale-Size-Dependent Magnetospheric Coupling, Journal of Geophysical Research: Space Physics, 95, 15 157–15 166, https://doi.org/10.1029/JA095iA09p15157, 1990.

Kintner P. M., Ledvina B. M., and de Paula E. R.: GPS and Ionospheric Scintillations, Space Weather, 5, https://doi.org/10.1029/2006SW000260, 2007.

Kivanc and Heelis, R. A.: Spatial Distribution of Ionospheric Plasma and Field Structures in the High-Latitude F Region, Journal of Geophysical Research, 103, 6955–6968, https://doi.org/10.1029/97JA03237, 1998.

430 Knudsen, D. J., Kelley, M. C., Earle, G. D., Vickrey, J. F., and Boehm, M.: Distinguishing Alfvén Waves from Quasi-Static Field Structures Associated with the Discrete Aurora: Sounding Rocket and HILAT Satellite Measurements, Geophysical Research Letters, 17, 921–924, https://doi.org/10.1029/GL017i007p00921, 1990.

Krämer, E., Koller, F., Suni, J., LaMoury, A. T., Pöppelwerth, A., Glebe, G., Mohammed-Amin, T., Raptis, S., Vuorinen, L., Weiss, S., Xirogiannopoulou, N., Archer, M., Blanco-Cano, X., Gunell, H., Hietala, H., Karlsson, T., Plaschke, F., Preisser, L., Roberts, O., Si-
435 mon Wedlund, C., Temmer, M., and Vörös, Z.: Jets Downstream of Collisionless Shocks: Recent Discoveries and Challenges, Space Science Reviews, 221, 4, https://doi.org/10.1007/s11214-024-01129-3, 2024.

Kwak, Y.-S. and Richmond, A. D.: An Analysis of the Momentum Forcing in the High-Latitude Lower Thermosphere, Journal of Geophysical Research: Space Physics, 112, https://doi.org/10.1029/2006JA011910, 2007.

La Rosa, B. H. and Hysell, D. L.: Modeling and Analysis of Artificial Periodic Inhomogeneities in the Ionosphere, Radio Science, 60,
440 e2025RS008 226, https://doi.org/10.1029/2025RS008226, 2025.

Li, Q., Liu, L., Jiang, J., Li, W., Huang, H., Yu, Y., Li, J., Zhang, R., Le, H., and Chen, Y.: Alpha-Chapman Scale Height: Longitudinal Variation and Global Modeling, Journal of Geophysical Research: Space Physics, 124, 2083–2098, https://doi.org/10.1029/2018JA026286, 2019.

Lysak, R.: Feedback Instability of the Ionospheric Resonant Cavity, https://doi.org/10.1029/90JA02154, 1991.

445 Lysak, R., Echim, M., Karlsson, T., Marghitu, O., Rankin, R., Song, Y., and Watanabe, T.-H.: Quiet, Discrete Auroral Arcs: Acceleration Mechanisms, Space Science Reviews, 216, 92, https://doi.org/10.1007/s11214-020-00715-5, 2020.

Madhanakumar, M., Spicher, A., Vierinen, J., and Oksavik, K.: On the Strength of E and F Region Irregularities for GNSS Scintillation in the Dayside Polar Ionosphere, Journal of Atmospheric and Solar-Terrestrial Physics, 256, 106 197, https://doi.org/10.1016/j.jastp.2024.106197, 2024.

450 McCaffrey, A. M. and Jayachandran, P. T.: Determination of the Refractive Contribution to GPS Phase "Scintillation", Journal of Geophysical Research: Space Physics, 124, 1454–1469, https://doi.org/10.1029/2018JA025759, 2019.

Meziane, K., Hamza, A. M., and Jayachandran, P. T.: Turbulence Signatures in High-Latitude Ionospheric Scintillation, Journal of Geophysical Research: Space Physics, 128, e2022JA030 934, https://doi.org/10.1029/2022JA030934, 2023.

Moen, J. and Brekke, A.: The Solar Flux Influence on Quiet Time Conductances in the Auroral Ionosphere, Geophysical Research Letters,
455 20, 971–974, https://doi.org/10.1029/92GL02109, 1993.

Moisan, M. and Pelletier, J.: Hydrodynamic Description of a Plasma, in: Physics of Collisional Plasmas: Introduction to High-Frequency Discharges, edited by Moisan, M. and Pelletier, J., pp. 203–335, Springer Netherlands, Dordrecht, https://doi.org/10.1007/978-94-007-4558-2_3, 2012.

Newell, P. T. and Meng, C.-I.: The Cusp and the Cleft/Boundary Layer: Low-altitude Identification and Statistical Local Time Variation,
460 Journal of Geophysical Research: Space Physics, 93, 14 549–14 556, https://doi.org/10.1029/JA093iA12p14549, 1988.

Newell, P. T., Sotirelis, T., and Wing, S.: Diffuse, Monoenergetic, and Broadband Aurora: The Global Precipitation Budget, Journal of Geophysical Research: Space Physics, 114, https://doi.org/10.1029/2009JA014326, 2009.

Newell, P. T., Sotirelis, T., and Wing, S.: Seasonal Variations in Diffuse, Monoenergetic, and Broadband Aurora, Journal of Geophysical Research: Space Physics, 115, https://doi.org/10.1029/2009JA014805, 2010.

465 Ni, B., Bortnik, J., Nishimura, Y., Thorne, R. M., Li, W., Angelopoulos, V., Ebihara, Y., and Weatherwax, A. T.: Chorus Wave Scattering Responsible for the Earth's Dayside Diffuse Auroral Precipitation: A Detailed Case Study, Journal of Geophysical Research: Space Physics, 119, 897–908, https://doi.org/10.1002/2013JA019507, 2014.

Nishimura, Y., Bortnik, J., Li, W., Thorne, R. M., Ni, B., Lyons, L. R., Angelopoulos, V., Ebihara, Y., Bonnell, J. W., Le Contel, O., and Auster, U.: Structures of Dayside Whistler-Mode Waves Deduced from Conjugate Diffuse Aurora, Journal of Geophysical Research: Space Physics, 118, 664–673, https://doi.org/10.1029/2012JA018242, 2013.

Picone, J. M., Hedin, A. E., Drob, D. P., and Aikin, A. C.: NRLMSISE-00 Empirical Model of the Atmosphere: Statistical Comparisons and Scientific Issues, Journal of Geophysical Research: Space Physics, 107, SIA 15–1–SIA 15–16, https://doi.org/10.1029/2002JA009430, 2002.

Prölss, G. W.: Absorption and Dissipation of Solar Radiation Energy, in: Physics of the Earth's Space Environment: An Introduction, edited by Prölss, G. W., pp. 77–157, Springer, Berlin, Heidelberg, https://doi.org/10.1007/978-3-642-97123-5_3, 2004a.

Prölss, G. W.: Absorption and Dissipation of Solar Wind Energy, in: Physics of the Earth's Space Environment: An Introduction, edited by Prölss, G. W., pp. 349–399, Springer, Berlin, Heidelberg, https://doi.org/10.1007/978-3-642-97123-5_7, 2004b.

Redmon, R. J., Denig, W. F., Kilcommons, L. M., and Knipp, D. J.: New DMSP Database of Precipitating Auroral Electrons and Ions, Journal of geophysical research. Space physics, 122, 9056–9067, https://doi.org/10.1002/2016JA023339, 2017.

Rinnert, K.: Plasma Waves Observed in the Auroral E-region - ROSE Campaign, Journal of Atmospheric and Terrestrial Physics, 54, 683–692, https://doi.org/10.1016/0021-9169(92)90106-U, 1992.

Robinson, R. M., Zanetti, L., Anderson, B., Vines, S., and Gjerloev, J.: Determination of Auroral Electrodynamic Parameters From AMPERE Field-Aligned Current Measurements, Space Weather, 19, e2020SW002 677, https://doi.org/10.1029/2020SW002677, 2021.

Schunk, R. W. and Nagy, A. F.: Ionospheres of the Terrestrial Planets, Reviews of Geophysics, 18, 813–852, https://doi.org/10.1029/RG018i004p00813, 1980.

Sheehan, C. H. and St.-Maurice, J.-P.: Dissociative Recombination of N2+, O2+, and NO+: Rate Coefficients for Ground State and Vibrationally Excited Ions, Journal of Geophysical Research: Space Physics, 109, https://doi.org/10.1029/2003JA010132, 2004.

Shen, Y., Verkhoglyadova, O. P., Artemyev, A., Hartinger, M. D., Angelopoulos, V., Shi, X., and Zou, Y.: Magnetospheric Control of Ionospheric TEC Perturbations via Whistler-Mode and ULF Waves, AGU Advances, 5, e2024AV001 302, https://doi.org/10.1029/2024AV001302, 2024.

Sibeck, D. G. and Murphy, K. R.: Quantifying the Effects of Solar Wind Fluctuations on the Solar Wind-Magnetosphere Interaction, Geophysical Research Letters, 52, e2025GL114 954, https://doi.org/10.1029/2025GL114954, 2025.

Song, K., Hamza, A. M., Jayachandran, P. T., Meziane, K., and Kashcheyev, A.: Spectral Characteristics of Phase Fluctuations at High Latitude, Journal of Geophysical Research: Space Physics, 128, e2022JA031 244, https://doi.org/10.1029/2022JA031244, 2023.

Spasojevic, M. and Inan, U. S.: Drivers of Chorus in the Outer Dayside Magnetosphere, Journal of Geophysical Research: Space Physics, 115, https://doi.org/10.1029/2009JA014452, 2010.

Spogli, L., Ghobadi, H., Cicone, A., Alfonsi, L., Cesaroni, C., Linty, N., Romano, V., and Cafaro, M.: Adaptive Phase Detrending for GNSS Scintillation Detection: A Case Study over Antarctica, IEEE Geoscience and Remote Sensing Letters, 19, 1–5, 2021.

St-Maurice, J.-P. and Goodwin, L.: Revisiting the Behavior of the E-Region Electron Temperature During Strong Electric Field Events at High Latitudes, Journal of Geophysical Research: Space Physics, 126, 2020JA028 288, https://doi.org/10.1029/2020JA028288, 2021.

Thébault, E., Finlay, C. C., Beggan, C. D., Alken, P., Aubert, J., Barrois, O., Bertrand, F., Bondar, T., Boness, A., Brocco, L., Canet, E., Chambodut, A., Chulliat, A., Coïsson, P., Civet, F., Du, A., Fournier, A., Fratter, I., Gillet, N., Hamilton, B., Hamoudi, M., Hulot, G., Jager, T., Korte, M., Kuang, W., Lalanne, X., Langlais, B., Léger, J.-M., Lesur, V., Lowes, F. J., Macmillan, S., Mandea, M., Manoj, C., Maus, S., Olsen, N., Petrov, V., Ridley, V., Rother, M., Sabaka, T. J., Saturnino, D., Schachtschneider, R., Sirol, O., Tangborn, A.,

Thomson, A., Tøffner-Clausen, L., Vigneron, P., Wardinski, I., and Zvereva, T.: International Geomagnetic Reference Field: The 12th Generation, Earth, Planets and Space, 67, 79, https://doi.org/10.1186/s40623-015-0228-9, 2015.

Thomas, E. G. and Shepherd, S. G.: Statistical Patterns of Ionospheric Convection Derived From Mid-latitude, High-Latitude, and Polar SuperDARN HF Radar Observations, Journal of Geophysical Research: Space Physics, 123, 3196–3216, https://doi.org/10.1002/2018JA025280, 2018.

Thorne, R. M., Ni, B., Tao, X., Horne, R. B., and Meredith, N. P.: Scattering by Chorus Waves as the Dominant Cause of Diffuse Auroral Precipitation, Nature, 467, 943–946, https://doi.org/10.1038/nature09467, 2010.

Tsunoda, R. T.: High-Latitude F Region Irregularities: A Review and Synthesis, Reviews of Geophysics, 26, 719–760, https://doi.org/10.1029/RG026i004p00719, 1988.

van der Meeren, C., Oksavik, K., Lorentzen, D., Moen, J. I., and Romano, V.: GPS Scintillation and Irregularities at the Front of an Ionization Tongue in the Nightside Polar Ionosphere, Journal of Geophysical Research: Space Physics, 119, 8624–8636, https://doi.org/10.1002/2014JA020114, 2014.

Vickrey, J. F. and Kelley, M. C.: The Effects of a Conducting E Layer on Classical F Region Cross-Field Plasma Diffusion, Journal of Geophysical Research: Space Physics, 87, 4461–4468, https://doi.org/10.1029/JA087iA06p04461, 1982.

Wang, Y., Zhang, Q.-H., Jayachandran, P. T., Moen, J., Xing, Z.-Y., Chadwick, R., Ma, Y.-Z., Ruohoniemi, J. M., and Lester, M.: Experimental Evidence on the Dependence of the Standard GPS Phase Scintillation Index on the Ionospheric Plasma Drift Around Noon Sector of the Polar Ionosphere, Journal of Geophysical Research: Space Physics, 123, 2370–2378, https://doi.org/10.1002/2017JA024805, 2018.

Wang, Y., Jayachandran, P. T., Ma, Y.-Z., Zhang, Q.-H., Xing, Z.-Y., Ruohoniemi, J. M., Shepherd, S. G., and Lester, M.: Dependencies of GPS Scintillation Indices on the Ionospheric Plasma Drift and Rate of Change of TEC Around the Dawn Sector of the Polar Ionosphere, Journal of Geophysical Research: Space Physics, 127, e2022JA030 870, https://doi.org/10.1029/2022JA030870, 2022.

Watanabe, T.-H., Fujita, K., and Maeyama, S.: Growth of Auroral Structures, Vortex Formation, Turbulence Transition, and Energy Cascade in Alfvénic Magnetosphere-Ionosphere Coupling, Geophysical Research Letters, 52, e2025GL118 354, https://doi.org/10.1029/2025GL118354, 2025.

Wiltberger, M., Merkin, V., Zhang, B., Toffoletto, F., Oppenheim, M., Wang, W., Lyon, J. G., Liu, J., Dimant, Y., Sitnov, M. I., and Stephens, G. K.: Effects of Electrojet Turbulence on a Magnetosphere-Ionosphere Simulation of a Geomagnetic Storm, Journal of Geophysical Research: Space Physics, 122, 5008–5027, https://doi.org/10.1002/2016JA023700, 2017.

Wood, A. G. and Pryse, S. E.: Seasonal Influence on Polar Cap Patches in the High-Latitude Nightside Ionosphere, Journal of Geophysical Research: Space Physics, 115, https://doi.org/10.1029/2009JA014985, 2010.

Yeh, K. C. and Liu, C.-H.: Radio Wave Scintillations in the Ionosphere, IEEE Proceedings, 70, 324–360, 1982.